

Conference Paper

Calculation of Field Characteristics in Periodic Nanostructures from Composite Elements with Activated Plasmon Modes

M.G.KUCHERENKO, A.P.RUSINOV, and D.A.KISLOV

Orenburg State University – Russia

Abstract

Modeling of the electromagnetic field of the optical frequency in periodic structures composed of parallel conducting nanorods as well as composite spherical nanoparticles with an excitonogenic envelope in hexagonal 2d-lattices - in the quasistatic approximation and the FDTD method. The qualitative agreement of these approaches is shown when calculating field characteristics in lattices of cylindrical elements.

Corresponding Author:

M.G.KUCHERENKO
clibph@yandex.ru

Received: 28 January 2018

Accepted: 15 March 2018

Published: 25 April 2018

Publishing services provided by
Knowledge E

© M.G.KUCHERENKO et al. This article is distributed under the terms of the [Creative Commons Attribution License](#), which permits unrestricted use and redistribution provided that the original author and source are credited.

Selection and Peer-review under the responsibility of the PhIO Conference Committee.

1. INTRODUCTION

Deposition of ultrathin (island) layers of metal on the dielectric surface significantly changes its properties, incl. and optical. Theoretically, this can be related to the behavior of the electron gas of nanoparticles in external electric and magnetic fields. Thus, in a homogeneous electromagnetic field of the optical frequency, plasmon oscillations of the electron density are excited in the conducting nanoparticles, as a result of which the near field near the surface of the particles changes [1-3]. It is obvious that in a system with a large number of particles, it is necessary to take into account their mutual influence on each other [4-5]. In the case of a regular spatial arrangement of particles, this calculation is quite simple.

Nanolattices have a number of properties that make them promising for use as elements of a new generation of miniature biosensors and compact optical radiation control elements. Anomalous transmission [6], anomalous opacity (non-transparency) [7], artificial optical and magneto-optical [8] activity, as well as the possibility of plasmon focusing [9-13] are described in the literature. The development of compact optoelectronic sensors is closely related to the need to obtain reproducible resonance characteristics in the interesting part of the spectrum.

OPEN ACCESS

In the first part of the paper, the field structure was studied in a quasistatic approximation and the probabilities of induced transitions of molecules located in a regular lattice of long parallel conducting rods of nanometer radius were calculated.

2. REGULAR GRATINGS COMPOSED FROM LONG CONDUCTIVE NANORODS (QUASISTATIC APPROXIMATION)

We orient the z axis of the Cartesian coordinate system along the axis of the lattice nanorods, and choose the direction of the external electric field \mathbf{E}_0 along the x axis perpendicular to z (Fig. 1), then the resulting field $E(r)$ will be the sum of the external field E_0 and the field of polarized rods [17], and the distribution $E(r)$ reduces to a picture in the (x, y) plane.

We introduce the vector $P_2(\omega)$ of the *dipole moment* of a unit length of a single nanorod of radius R by the relation

$$P_2(\omega) = \alpha_0(\omega)E_0.$$

Here

$$\alpha_0(\omega) = \frac{R^2 \varepsilon(\omega) - \varepsilon_m}{2 \varepsilon(\omega) + \varepsilon_m}; \varepsilon(\omega) = 1 - \frac{\omega_p^2}{\omega(\omega + i\gamma)}; \omega_p = \sqrt{\frac{4\pi e^2 n_e}{m}}$$

- is polarizability of unit length of nanorod, the dielectric constant and the plasma frequency of the metal, respectively.

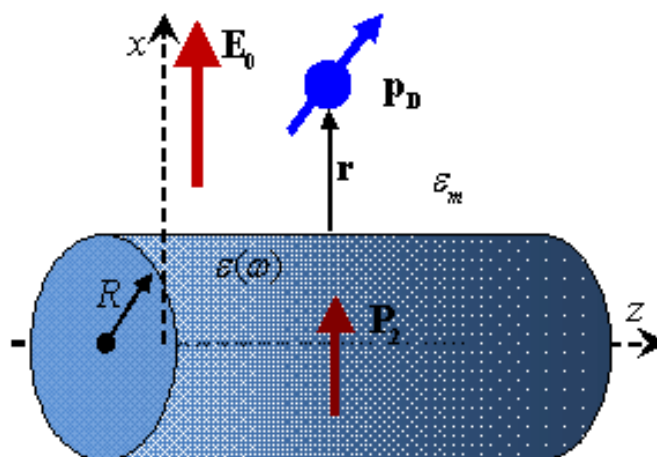


Figure 1: To the calculation of the local field of a metal nanorod of radius R in a medium with dielectric permittivity ε_m .

Potential of the summary near field outside the nanorod is given by expression

$$\phi(r) = -E_0 r + 2 \frac{P_2(\omega)r}{r^2},$$

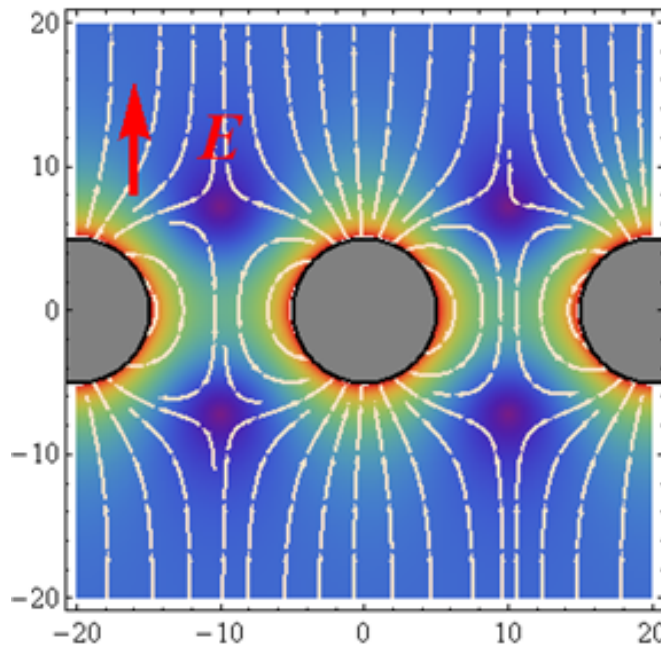


Figure 2: The near field structure of parallel nanorods and its relative amplitude $|E(r)|/E_0$.

and the field strength (Fig. 1) is given by expression

$$E(r) = -grad\phi(r) = E_0 - \vec{\nabla} \left(2 \frac{P_2(\omega)r}{r^2} \right).$$

In the case of regular spatial arrangement of parallel nanorods in the form of one-dimensional chain or two-dimensional grating, the effective dipole moment of unit length of each rod can be represented as $P_2(\omega) = \vec{\alpha}_{eff} E_0$, where the effective polarizability

$$\vec{\alpha}_{eff} = \left[\vec{I} - \alpha_0 \sum_i \sum_j \vec{G}(r_{ij}) \right]^{-1} \alpha_0, \tag{1}$$

and the dyadic quasistatic Green's function $\vec{G}(r)$, is a tensor of the second rank

$$\vec{G}(r) = \frac{1}{r^2} \left[2 \frac{r \otimes r}{r^2} - \vec{I} \right], \tag{2}$$

$r_{ij} = r + ie_1 + je_2$ is the radius vector of rod with indices i and j , e_1 and e_2 are the elementary vectors of two-dimensional periodic nanorods lattice.

The field potential in such lattice is given by

$$\phi(r) = -E_0 r + 2 \sum_i \sum_j P_2(\omega) r_{ij} \frac{1}{r_{ij}^2}. \tag{3}$$

It can be seen from (1) and (2) that more distant conductors contribute less to both the effective polarizability of each rod and the total field potential at a given point.

Therefore, in practical calculations it is sufficient to take into account the influence of several nearest conductors.

For quasi-one-dimensional chain of parallel rods, one of the elementary vectors becomes infinite and summation over the corresponding index is not carried out. Numerical calculations show that the characteristics of the field of parallel chain of nanorods depend on the orientation of the vector \mathbf{E}_0 . Therefore, the local distortions of the field have the largest amplitude with orientation \mathbf{E}_0 across the axis of chain (Fig.2).

In quasi-two-dimensional geometry, calculations were performed for gratings with square $|e_1| = |e_2|$, $\angle(e_1e_2) = \pi/2$ and hexagonal $|e_1| = |e_2|$, $\angle(e_1e_2) = \pi/3$ packing of rods (Fig. 3).

Because of the known symmetry of these gratings, the resulting field in them depends periodically on vector \mathbf{E}_0 orientation. For the case of rectangular package, this dependence is repeated through an angle $\pi/4$, and for hexagonal packing – through $\pi/6$. The maximum local distortions of the field occur when vector \mathbf{E}_0 is oriented along vectors \mathbf{e}_1 and \mathbf{e}_2 of structure.

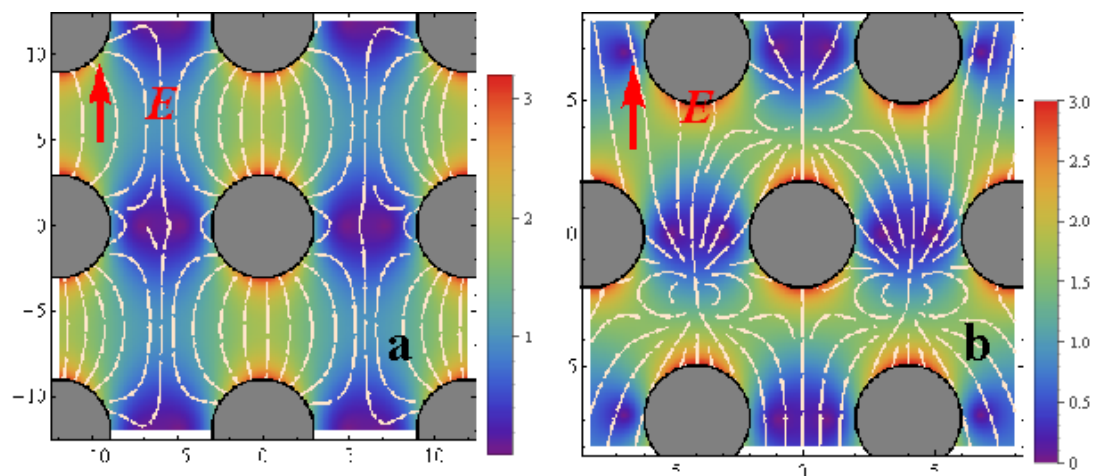


Figure 3: Field structure $E(r)$ and its relative amplitude $|E(r)|/E_0$ in the quasi-two-dimensional matrix of infinite nanorods for their square (a) and hexagonal (b) packing.

Simulation also shows that as the size of the system increases, the amplitude values of the local field distortion decrease, and the spatial dimensions of such regions increase. In this case, along the direction of the vector \mathbf{E}_0 , co-directed with the lattice vector \mathbf{e}_1 , the energy density of the field is concentrated near the nanorods, and in the transverse direction the maximum of the field is located between them.

It is shown that in calculating the probability of induced transitions for a molecule in nanorods lattice, it is necessary to take into account the orientation of its transition

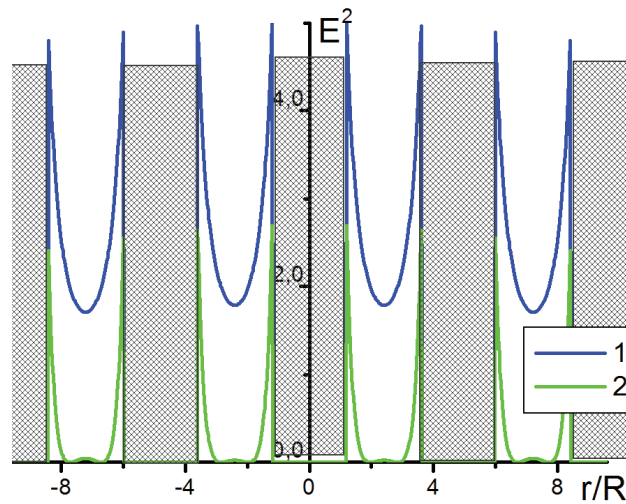


Figure 4: Field intensity in square gratings of nanorods along the lines passing through them and co-directed with vectors \mathbf{e}_1 (1) and \mathbf{e}_2 (2) of lattice решетки.

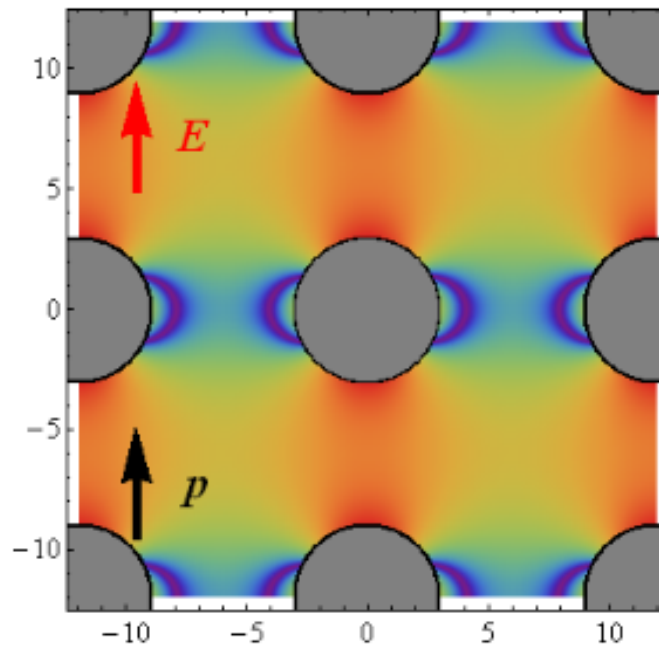


Figure 5: Logarithm of relative transition probability in square lattice from nanorods $(p_D E(r))^2 / (p_0 E_0)^2$ under the collinear orientation of $p_D \uparrow E_0$ vectors.

dipole moment p_D , both with respect to the orientation of the external field \mathbf{E}_0 and relative to the principal axes of the quasi-two-dimensional structure. The case of a coincident orientation of the vectors $p_D \uparrow E_0$ is indicative (Fig. 5), since their transition probability decreases with their angular misalignment.

3. POLARIZATION PROPERTIES OF NANOLATTICES COMPOSED FROM SPHERICAL LAYER COMPOSITES WITH EXCITONOGENEOUS SHELL AND MAGNETIZED METAL CORE

3.1. Polarizability of a particle in a planar lattice in the approximation of the first two coordination spheres

Let us now consider the aggregate of nanoparticles forming an infinite planar lattice of hexagonal symmetry. We will calculate the interaction of polarized nanoparticles in the approximation of the first two coordination spheres, as shown in Figure 6. The effect of particles in other coordination spheres is not taken into account, because their contribution to the polarizability of the particle in question will be negligibly small.

Since such a system is symmetric, the induced polarizability will be the same on all particles of the infinite lattice. Then taking into account the six nearest neighbors of the first coordination sphere and the twelve dipoles of the second coordination sphere in the lattice gives the following expression for the dipole moment vector of the isolated nanoparticle

$$\begin{aligned}
 P_2(\omega) = & \alpha_0 \left[E_0 + \vec{G}_1(a)P_2(\omega) + \vec{G}_2(a)P_2(\omega) + \dots + \vec{G}_6(a)P_2(\omega) \right] + \\
 & + \alpha_0 \left[\vec{G}_7(2a)P_2(\omega) + \vec{G}_9(2a)P_2(\omega) + \dots + \vec{G}_{17}(2a)P_2(\omega) \right] + \\
 & + \alpha_0 \left[\vec{G}_8(2h)P_2(\omega) + \vec{G}_{10}(2h)P_2(\omega) + \dots + \vec{G}_{18}(2h)P_2(\omega) \right] +
 \end{aligned} \tag{4}$$

Here α_0 is the polarizability of a single nanoparticle; $h = a\sqrt{3}/2$, a - distance between neighboring particles; $\vec{G}(r)$ - the three-dimensional Green's tensor, in contrast to (2) defined by the relation

$$\vec{G}_j(r) = \frac{1}{r^3}(3n \otimes n - I) \tag{5}$$

Otherwise, by regrouping the terms in (4), we obtain

$$\left[I - \alpha_0 \left(\sum_{j=1}^6 \vec{G}_j(a) + \sum_{j=3}^8 \vec{G}_{2j+1}(2a) + \sum_{j=4}^9 \vec{G}_{2j}(2h) \right) \right] P_2(\omega) = \alpha_0 E_0. \tag{6}$$

Then the effective polarizability tensor of a spherical nanocomposite in a lattice in the approximation of the two first coordination spheres can be written in the form

$$\vec{\alpha}_{\text{eff}}(\omega) = \left[I - \alpha_0(\omega) \left(\sum_{j=1}^6 \vec{G}_j(a) + \sum_{j=3}^8 \vec{G}_{2j+1}(2a) + \sum_{j=4}^9 \vec{G}_{2j}(2h) \right) \right]^{-1} \alpha_0(\omega). \tag{7}$$

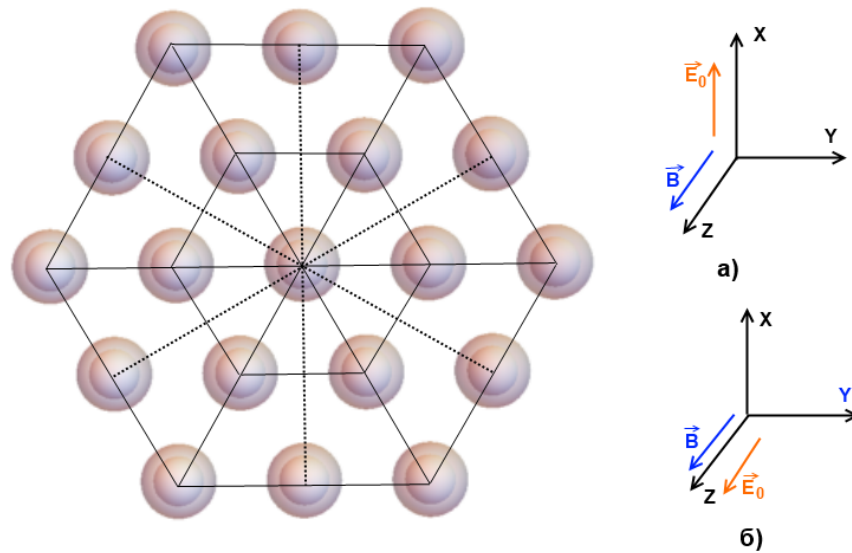


Figure 6: The first two coordination spheres of a planar lattice of layered spherical nanocomposites. To the calculation of a) transverse, b) longitudinal polarizability.

For the dipole polarizability tensor $\vec{\alpha}_0$ of a spherical layered composite with an anisotropic core, owing to the superposition of an external magnetic field of induction \mathbf{B} , the following expression was obtained previously [3]

$$\begin{aligned} & \vec{A}(\vec{\epsilon}_1(\omega | \mathbf{B}), \epsilon_2, \epsilon_3) \\ &= \left[(\vec{\epsilon}_1(\omega | \mathbf{B}) + 2\epsilon_2)(\epsilon_2 - \epsilon_3) + (\vec{\epsilon}_1(\omega | \mathbf{B}) - \epsilon_2)(2\epsilon_2 + \epsilon_3)\xi^3 \right] \times \quad (8) \\ & \times \left[(\vec{\epsilon}_1(\omega | \mathbf{B}) + 2\epsilon_2)(\epsilon_2 + 2\epsilon_3) + 2(\vec{\epsilon}_1(\omega | \mathbf{B}) - \epsilon_2)(\epsilon_2 - \epsilon_3)\xi^3 \right]^{-1} R_2^3, \end{aligned}$$

Here $\xi = R_1/R_2$ is the ratio of the core radius to the outer radius of the spherical composite. $\epsilon(\omega)$, $\epsilon_2(\omega)$, ϵ_3 - dielectric permittivities of the metal core, excitonogenic shell and external environment, respectively. When the magnetic field is turned off, all tensor quantities appearing in (8) are reduced to their scalar prototypes and expression (8) is transformed to the known expression [2, 17] for the polarizability of an isotropic composite.

The components of the tensor $\alpha_{\text{eff}}^{1,1}(\omega) = \alpha_{\text{eff}}^{2,2}(\omega)$ will correspond to the transverse polarizability, as shown in Fig. 6a, and the component $\alpha_{\text{eff}}^{3,3}(\omega)$ - longitudinal polarizability, as shown in Fig. 6b.

Below, in Figures 7 and 8, the spectra of imaginary and real parts of the polarizabilities of a separate layered nanoparticle and a layered nanoparticle that forms part of a planar lattice are presented. It is seen from the graphs that for the transverse

polarizability of the nanoparticle in the lattice, the resonances will shift to the low-frequency region, and for the longitudinal polarizability to the high-frequency region of the spectrum relative to the polarizability resonances of the isolated nanocomposite. In this case, the amplitudes of the exciton resonances of the transverse polarizability $\alpha_{\text{eff}}^{1,1}(\omega)$ will be larger, and the amplitudes of the exciton resonances of the longitudinal polarizability $\alpha_{\text{eff}}^{3,3}(\omega)$ are smaller. The amplitudes of plasmon resonances are practically the same for all three types of polarizabilities under consideration.

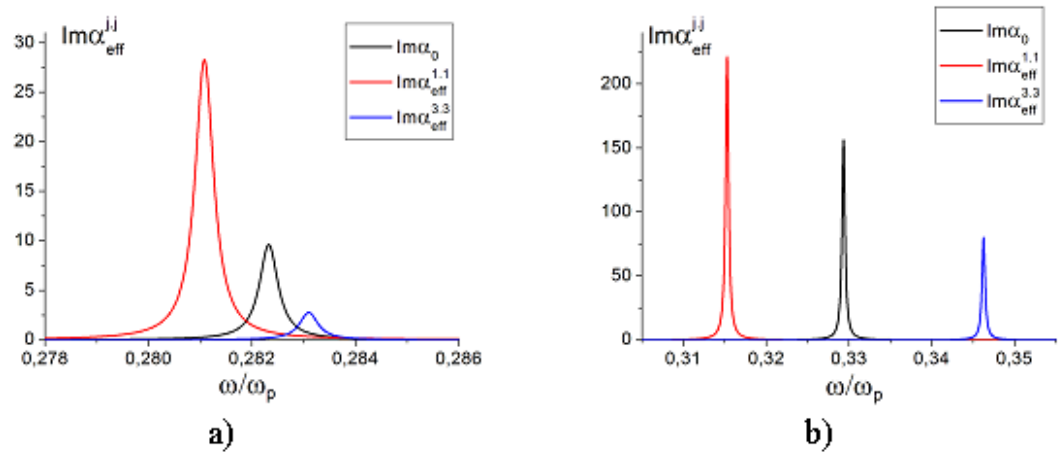


Figure 7: Comparison of the exciton bands of the imaginary parts of the polarizability of a separate layered spherical nanoparticle, the transverse $\text{Im}\alpha_{\text{eff}}^{1,1}(\omega)$ and $\text{Im}\alpha_{\text{eff}}^{3,3}(\omega)$ longitudinal polarizabilities of a layered nanoparticle in a planar lattice a) low-frequency and b) high-frequency exciton resonances. $R_1 = 60$ nm, $R_2 = 80$ nm, $\gamma = 6 \cdot 10^{12} \text{ c}^{-1}$, $a = 180$ nm, $\Gamma = 3 \cdot 10^{12} \text{ c}^{-1}$, $\omega_{\text{exc}} = 4 \cdot 10^{15} \text{ c}^{-1}$.

In a magnetic field, the amplitudes of all three resonances of the polarizability of a layered nanoparticle in a planar lattice decrease, and plasmon resonance, in addition, splits into two spectral components that expand with increasing magnetic induction B , just as in the case of a separate nanocomposite, as demonstrated in Fig. 9 and 10.

Thus, for a layered nanoparticle with an excitonogenic shell and a metal core located in a planar lattice of the same particles, the exciton and plasmon resonances are displaced, and the effect of the external magnetic field is analogous to the case of a solitary layered nanoparticle.

3.2. Comparison of the dipole polarizabilities of a separate layered nanocomposite with its lattice analog

Next, we compare the polarizability spectra of a separate layered nanocomposite $\alpha_0(\omega)$ and layered composites that form part of a flat and three-dimensional $\alpha_{3-d}(\omega)$ lattice.

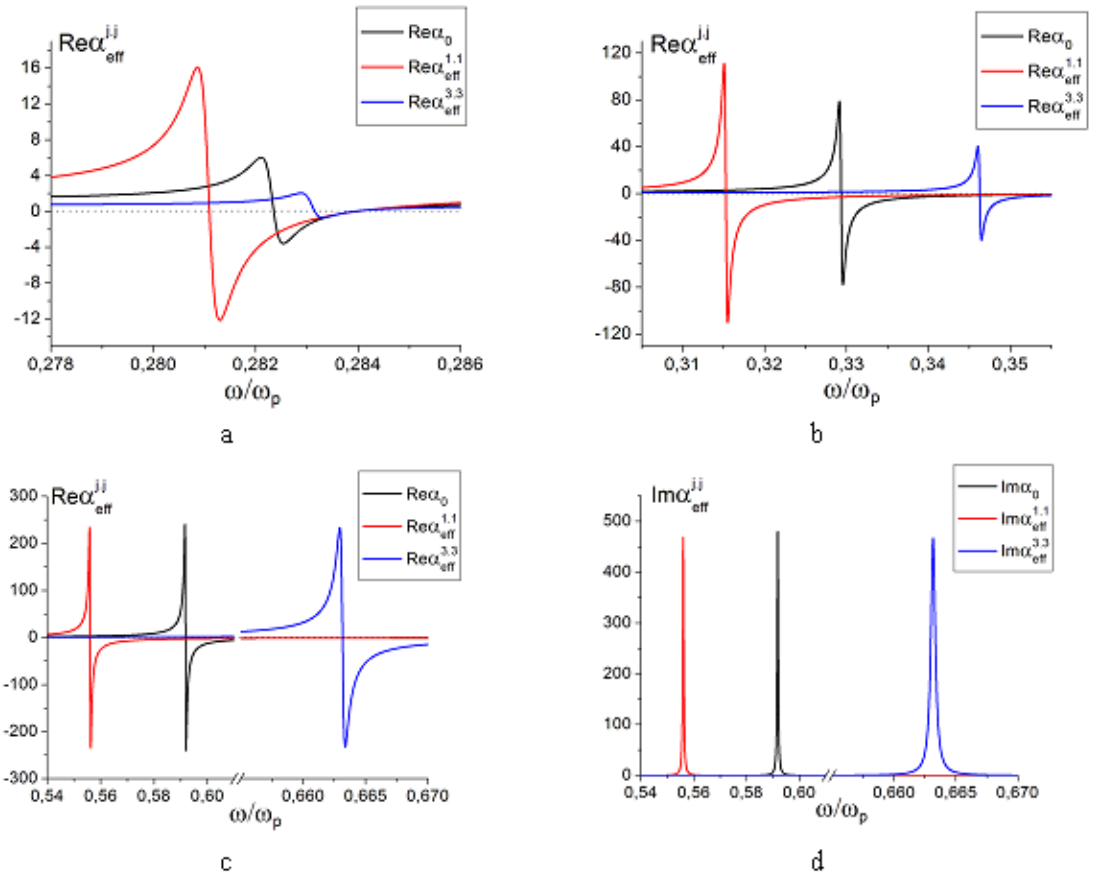


Figure 8: Comparison of the spectra of the polarizability α_0 of a separate layered spherical nanoparticle, the transverse $\alpha_{\text{eff}}^{1,1}$ and longitudinal $\alpha_{\text{eff}}^{3,3}$ polarizabilities of a nanoparticle in a planar lattice of layered nanocomposites a), b) exciton resonances (Re parts), c), d) plasmon resonances (Re and Im parts).

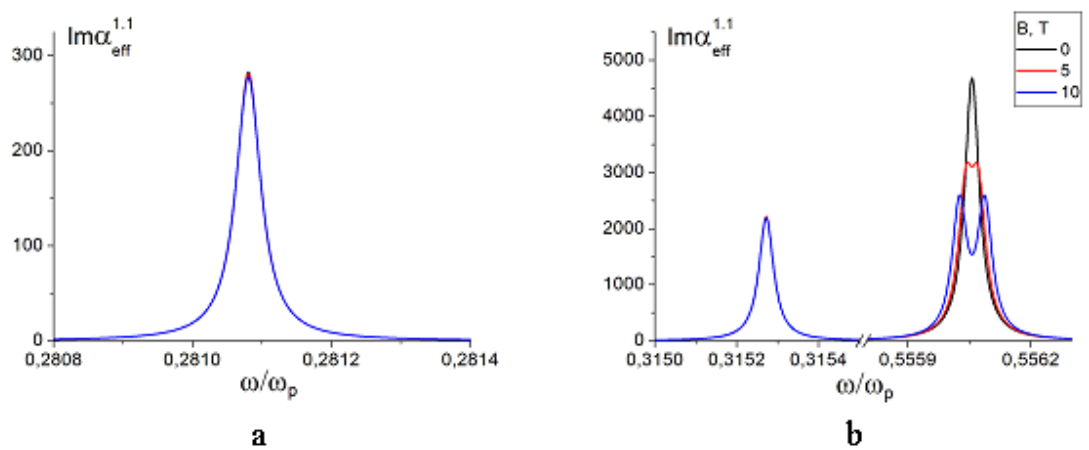


Figure 9: Spectra of the imaginary part of the transverse polarizability of a layered nanoparticle in a planar lattice of layered nanocomposites as a function of the magnitude of the magnetic induction B . a) exciton resonance, b) exciton and plasmon resonances. $R_1 = 60 \text{ nm}$, $R_2 = 80 \text{ nm}$, $\gamma = 6 \cdot 10^{11} \text{ c}^{-1}$, $a = 180 \text{ nm}$, $\Gamma = 3 \cdot 10^{11} \text{ c}^{-1}$, $\omega_{\text{exc}} = 4 \cdot 10^{15} \text{ c}^{-1}$.

As can be seen from Figures 11 and 12, resonances of the transverse polarizability $\alpha_{2-d}^{1,1}(\omega)$ of a layered nanocomposite in a planar lattice are shifted to a low-frequency

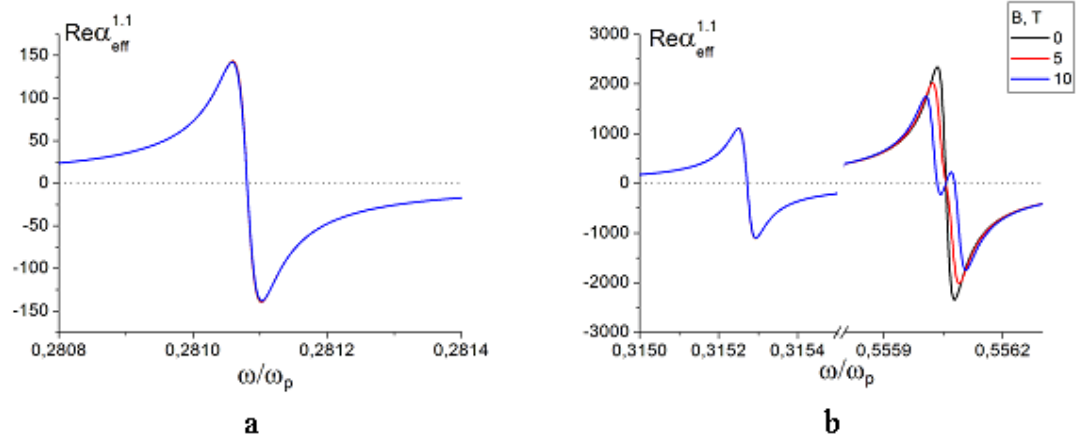


Figure 10: Spectra of the real part of the transverse polarizability $Re\alpha_{eff}^{1,1}$ of a layered nanocomposite of a particle in a planar lattice of identical elements, depending on the magnitude of the magnetic induction B . a) low-frequency exciton resonance, b) high-frequency exciton resonance and the plasmon resonance split in a magnetic field.

region, increasing in amplitude, and resonances of the transverse polarizability of a nanocomposite in a bulk lattice to the high-frequency region of the spectrum, decreasing in amplitude. However, it can be seen that the displacement of resonances of the polarizability of a nanoparticle in a planar lattice will be more pronounced. Obviously, this is due to the symmetry and dimensionality of the flat and volume lattices.

For resonances of the longitudinal polarizability of particles in a plane $\alpha_{2-d}^{3,3}(\omega)$ and volume $\alpha_{3-d}^{3,3}(\omega)$ lattice, the opposite effect is observed, as shown in Figures 13 and 14. Resonances of the longitudinal polarizability $\alpha_{2-d}^{3,3}(\omega)$ of a layered nanoparticle in a plane lattice decrease in amplitude and shift to a low-frequency region, and resonances of the longitudinal polarizability $\alpha_{3-d}^{3,3}(\omega)$ of the nanoparticle in the bulk lattice increase in amplitude and are shifted to the low-frequency region of the spectrum. But the displacement of resonances of the polarizability of a layered nanoparticle in a planar lattice is still as large as the displacement of resonances of the polarizability of a layered nanoparticle in a bulk lattice.

Thus, a comparison of the polarizability spectra of a separate layered nanocomposite and nanocomposites included in a planar and bulk lattice shows that the symmetry and dimension of such lattices cause a displacement of the resonances, which is more pronounced in the case of a planar lattice.

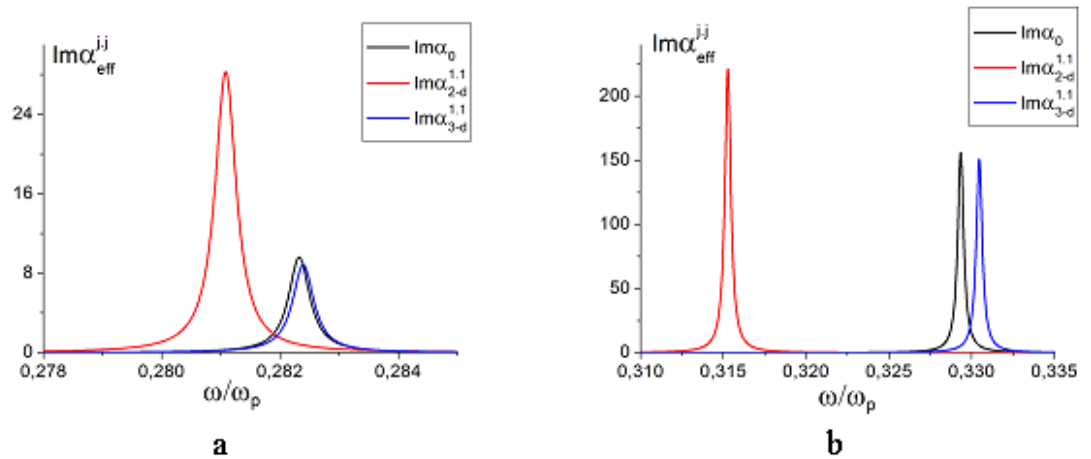


Figure 11: Comparison of the spectra of imaginary parts of the polarizability of a separate layered spherical nanoparticle $\text{Im } \alpha_0$ and transverse polarizabilities for layered nanoparticles in a plane $\text{Im } \alpha_{2-d}^{1,1}$ and bulk $\text{Im } \alpha_{3-d}^{1,1}$ lattice. Low-frequency (a), and high-frequency (b) exciton resonances. $R_1 = 60 \text{ nm}$, $R_2 = 80 \text{ nm}$, $B = 0 \text{ T}$, $\gamma = 6 \cdot 10^{12} \text{ c}^{-1}$, $a = 180 \text{ nm}$, $\Gamma = 3 \cdot 10^{12} \text{ c}^{-1}$, $\omega_p = 13,87 \cdot 10^{15} \text{ c}^{-1}$, $\omega_{exc} = 4 \cdot 10^{15} \text{ c}^{-1}$.

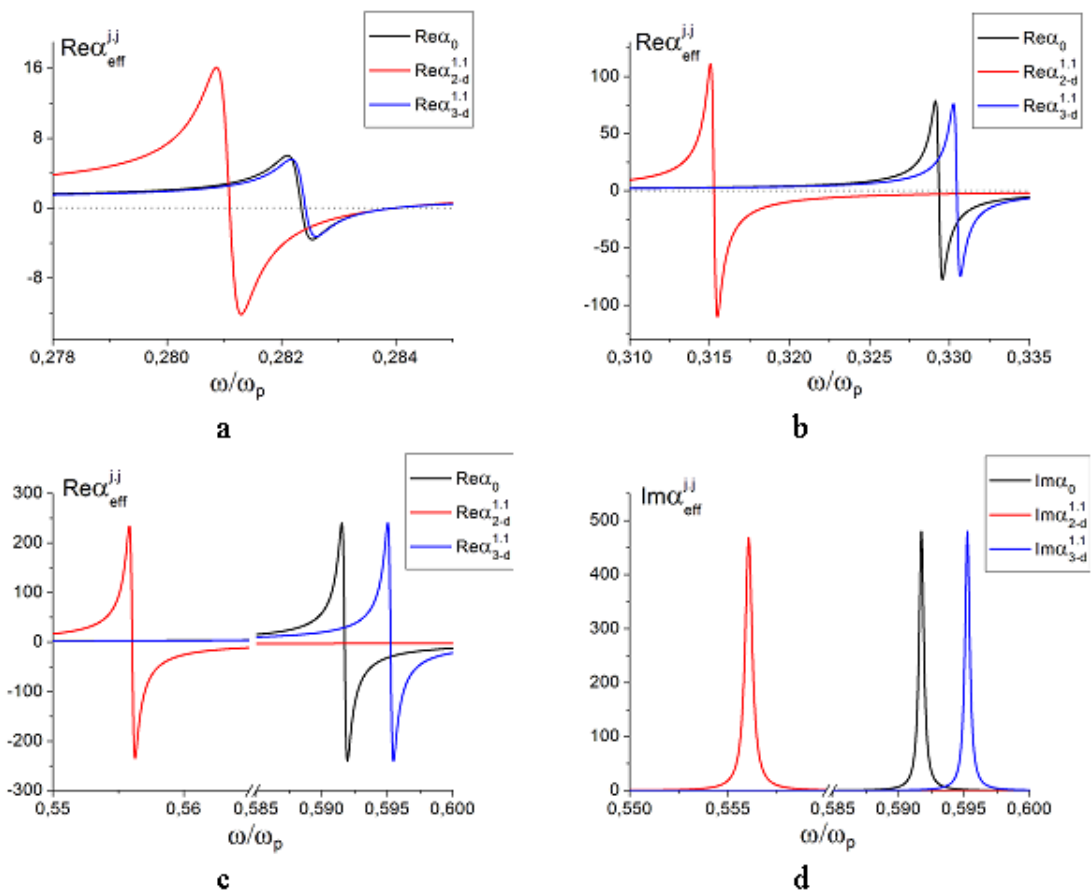


Figure 12: Comparison of the polarizability spectra of a separate layered spherical nanoparticle α_0 and transverse polarizabilities for layered nanoparticles in a plane $\alpha_{2-d}^{1,1}$ and bulk $\alpha_{3-d}^{1,1}$ lattice a), b) exciton resonances (Re parts); c), d) plasmon resonances (Re and Im parts).

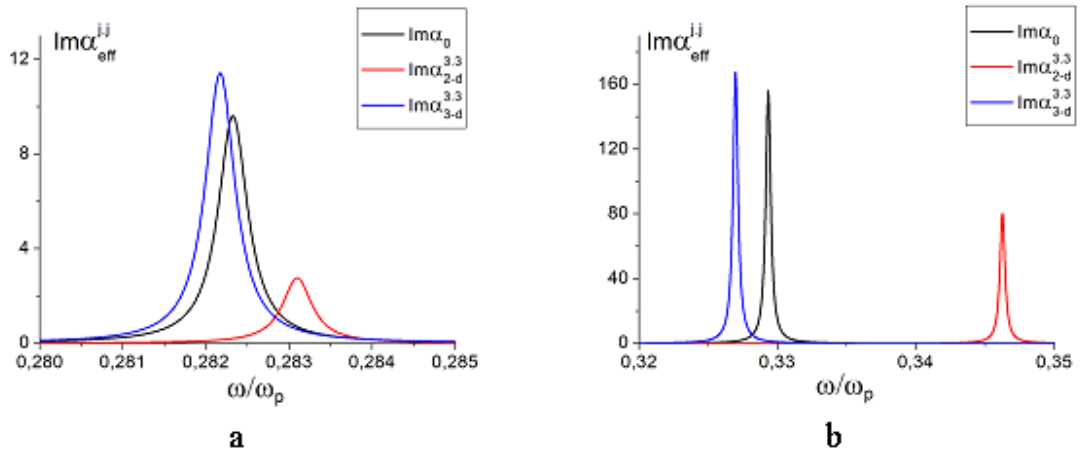


Figure 13: Comparison of the spectra of imaginary parts of the polarizability of a separate layered spherical nanoparticle $Im\alpha_0$ and longitudinal polarizabilities for layered nanoparticles in a plane $Im\alpha_{2-d}^{3,3}$ and bulk $Im\alpha_{3-d}^{3,3}$ lattice. a) low-frequency, b) high-frequency exciton resonances.

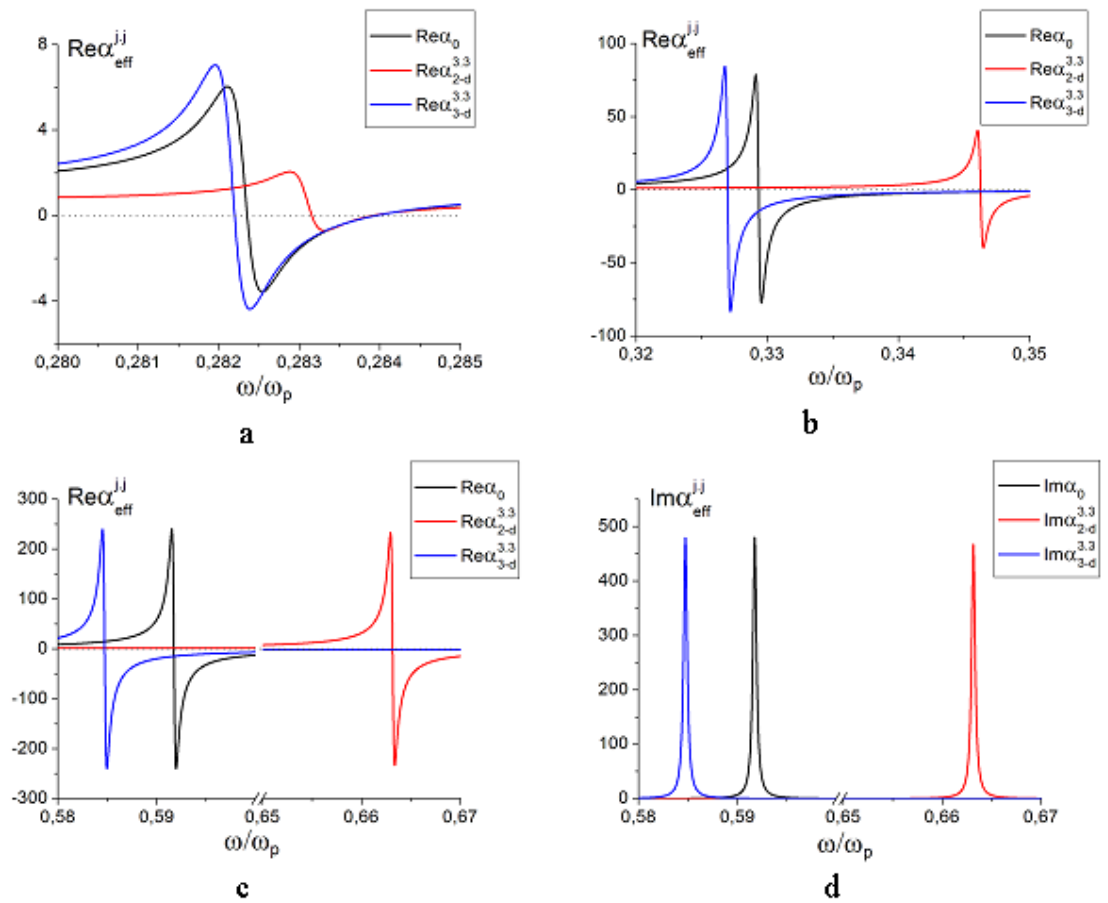


Figure 14: Comparison of the spectra of real parts of the polarizability of a separate layered spherical nanoparticle α_0 and longitudinal polarizabilities for layered nanoparticles in a plane $\alpha_{2-d}^{3,3}$ and bulk $\alpha_{3-d}^{3,3}$ lattice a) low-frequency and b) high-frequency exciton resonances (Re parts); c) Re and d) Im parts of polarizabilities - plasmon resonances

4. FDTD MODELING OF ELECTROMAGNETIC FIELD IN THE SQUARE LATTICE FROM NANOCYLINDERS

An alternative way to calculate the electromagnetic field can be a direct numerical solution of Maxwell's equations by the FDTD method [14]. One of the advantages of this method is the automatic accounting of the delay effect.

In this section, the spatial distribution of the electromagnetic field in periodic nanostructures composed of metal nanorods with activated plasmon modes was calculated by the FDTD method. Simulation was performed using the MEEP software package [14].

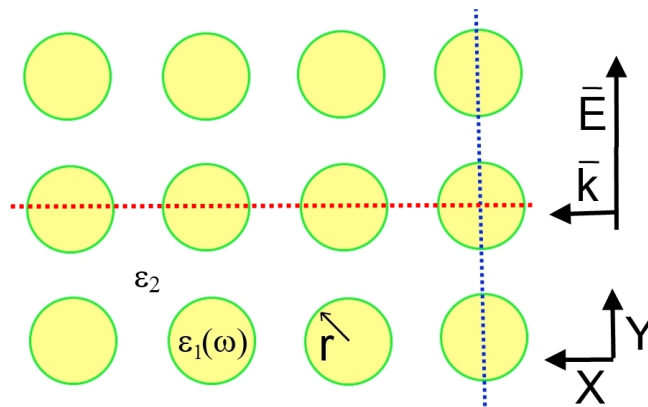


Figure 15: FDTD calculation scheme. The dashed lines show the cross sections in which the structure of the field is investigated.

For a numerical experiment, a two-dimensional countable domain was constructed. In this domain was a fragment of a square grating of nanorods. The scheme of the numerical experiment is shown in Figure 15. The axes of the nanorods were perpendicular to the counting domain. The radius of the nanocylinder was $r = 25$ nm, and its length is equal to infinity. The distance between the axes of two adjacent nanocylinders in the X direction was $3r$, in the Y direction was $4r$.

In the simulation, two types of nanocylinders were considered: from silver (Ag) and from silicon dioxide (SiO_2). The optical properties of the materials used in modeling were set by means of the dielectric permittivity $\epsilon_1(\omega)$. In this case, for silver, this function will be a frequency-dependent function (frequency dispersion), and for silicon dioxide a constant. It should be noted that in the FDTD method it is impossible to use the frequency-dependent permittivity in the form of a numbers table. Therefore, the dielectric properties of silver were approximated by the Drude-Lorentz model using experimental data [15, 16].

Calculations were made for two different external media with dielectric permittivity ϵ_2 : vacuum ($\epsilon_2 = 1$) and water ($\epsilon_2 = 1.77$).

A planar linearly polarized monochromatic wave with a wavelength $\lambda = 390$ nm (maximum of plasmon resonance in a silver nanocylinder in vacuum) was modeled as the initiating field. The plane of polarization of the electromagnetic wave coincides with the plane of the countable region (Fig. 15).

Figure 16 shows two-dimensional maps of the electric field average intensity spatial distribution in the interaction of an electromagnetic wave with nanocylinders in a square grating.

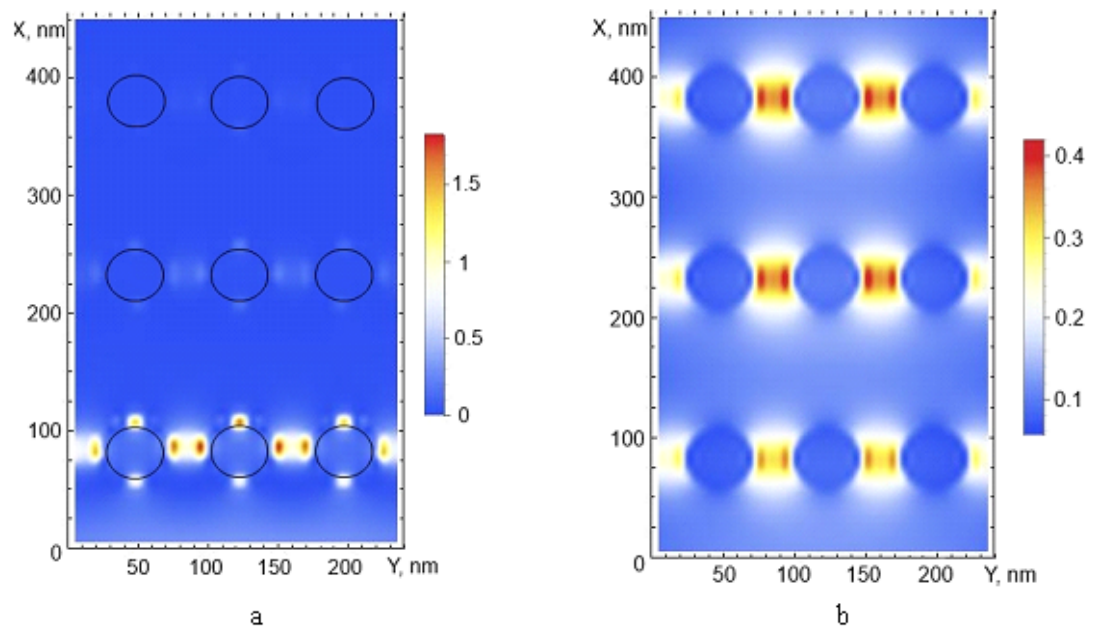


Figure 16: Time-averaged distribution of the intensity of the electric field in a rectangular grating of nanocylinders in a vacuum: a) Ag, b) SiO_2 .

It can be seen from Fig. 16a that the field structure in a medium with metallic nanorods is highly inhomogeneous. We see a lot of “hot spots”, where the field is locally amplified.

On the other hand, in Figure 16b for comparison, the distribution of the field is presented in the case when the grating is composed of nanocylinders without plasmon properties (SiO_2). It is seen that in this case the field is homogeneous.

Thus, it can be stated that the strong inhomogeneity of the field in the case of a metal grating is a manifestation of the plasmon properties of its constituent elements.

For a more detailed analysis of the field structure, we considered the average electric field intensity in two sections: along the vector \mathbf{E}_0 (blue dotted line in Fig. 15) and perpendicular to the vector \mathbf{E}_0 (red dotted line in Fig. 15).

Figure 17 shows the dependence of the electric field intensity in a rectangular grating of nanocylinders in the cross section along the vector \mathbf{E}_0 . It can be seen from the graphs that in the vacuum and in water the interaction of the electromagnetic wave with the grating occurs in different ways. This is evident from the structure of the field. It should be noted that the field is concentrated near the surface of the metal nanocylinder and is enhanced in comparison with the case when the grating consists of dielectric nanorods. In our case, the field intensity near the surface of the metal cylinder is approximately 5 times greater than the field intensity near the surface of the dielectric cylinder.

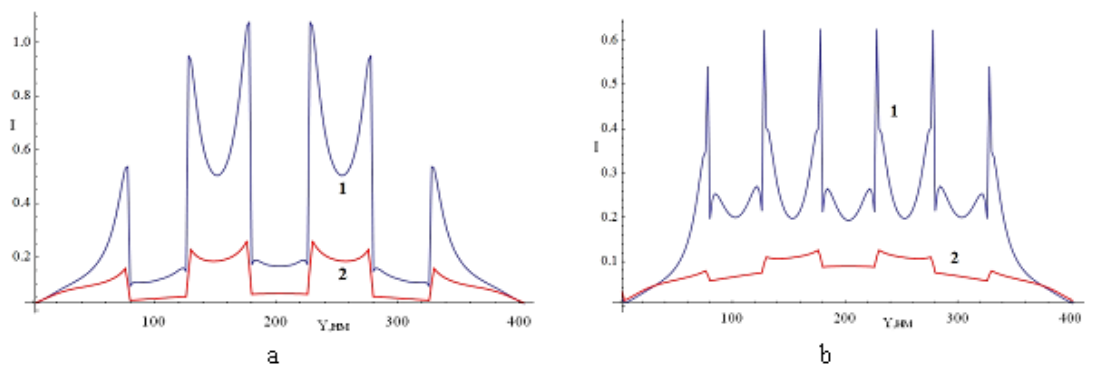


Figure 17: Dependence of the electric field intensity in a rectangular grating of nanocylinders in the cross section along the vector \mathbf{E}_0 (a - is vacuum, b - is water): 1-Ag, 2-SiO₂.

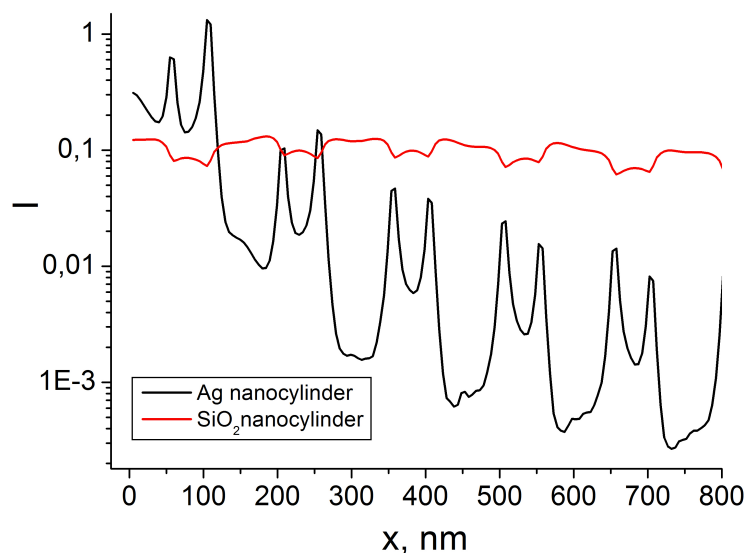


Figure 18: Dependence of the electric field intensity in a rectangular grating of nanocylinders in vacuum in a section perpendicular to the vector \mathbf{E}_0

Figure 18 shows the dependence of the electric field intensity in a rectangular grating of nanocylinders in a section perpendicular to the vector \mathbf{E}_0 .

It should be noted that, in contrast to the quasi-static model, the wave decays. In this figure, as in the previous, you can observe field amplification near the surface of

the conductive nanocylinders. In a grating of nanorods that do not possess plasmonic properties, the wave weakly decays and does not experience amplification.

It is seen from these dependences that the structure of a local field in a system of regular conducting nanocylinders calculated by different methods is qualitatively identical.

Acknowledgements

The authors acknowledge the support of The Ministry of Education and Science of Russia (№ 3.7758.2017/BP); the Russian Foundation for Basic Research (15-08-04132/17_a); Council President of the Russian Federation on grants for state support of young Russian scientists (SP-1340.2015.1). The authors are grateful to L.V. Terenina for assistance in the calculation of part 2.

References

- [1] Kucherenko M.G., Kislov D.A., Chmereva T. M. Possibilities of the Features Improvement for Scanning Nearfield Optical Microscope by Plasmon-Resonance Increasing of Radiationless Energy Transfer Rate // *Nanotechnologies in Russia*. 2012. -Vol. 7. -Nos. 3-4. -P. 196-204.
- [2] Klimov V. V., *Nanoplasmonics* [in Russian], Fizmatlit, Moscow (2009).
- [3] Kucherenko, M.G. Absorption and spontaneous emission of light by molecules near metal nanoparticles in external magnetic field / M.G. Kucherenko, V.M. Nalbandyan // *Physics Procedia* 73 (2015) 136 – 142. doi: 10.1016/j.phpro.2015.09.134 © 2015 The Authors. Published by Elsevier B.V.
- [4] Rechberger, W. Optical properties of two interacting gold nanoparticle/ W. Rechberger A. Hohenau, A. Leitner, J.R. Krenn, B. Lamprecht, F.R. Aussenegg // *Optics Communications*. -2003. -V.220. -P. 137-141.
- [5] Kucherenko, M.G., Nalbandyan, V.M. Dipole Polarizabilities and Absorption Cross Sections of Two-Particle Nanoclusters of Conductive Homogeneous and Layered Particles with the Degenerate Electron Gas // *Russian Physics Journal* 2017. 59 (9), c. 1425-1432
- [6] Ghaemi H.F. Thio Tineke, Grupp D.E., Ebbesen T.W., Lezec H.J. // *Phys. Rev. B* 58, 6779 - 6782 (1998).
- [7] Braun J., Gompf B., Kobiela G., and Dressel M. // *Phys. Rev. Lett.* 103, 203901 (2009).
- [8] Ctistis G., Papaioannou E., Patoka P. et. al. // *Nano Lett.*, v. 9, № 1, 2009.

- [9] Shantha Vedantam, Hyojune Lee, Japeck Tang et.al. // Nano Lett., v. 9, №. 10, 2009.
- [10] Fu Min Huang, Nikolay I. Zheludev // Nano Lett., v. 9, № 3, 2009.
- [11] Gilad M. Lerman, Avner Yanai, Uriel Levy // Nano Lett., v. 9, № 5, 2009.
- [12] Lieven Verslegers, Peter B. Catrysse, Zongfu Yu et. al. // Nano Lett., v. 9, № 1, 2009.
- [13] Weibin Chen, Don C. Abeysinghe, Robert L. Nelson, Qiwen Zhan // Nano Lett., v. 9, № 12, 2009.
- [14] <http://ab-initio.mit.edu/wiki/index.php/Meep>
- [15] Rakic A.D., Djurisis A.B., Elazar J.M., Majewski M.L., Optical properties of metallic films for vertical-cavity optoelectronic devices, Applied Optics. 37 (22) (1998) 5271-528.
- [16] Johnson P. B., Christy R. W., Optical Constants of the Noble Metals, Phys. Rev. B. 6 (1972) 4370-4379
- [17] Landau L.D. & Lifshitz E.M. Electrodynamics of Continuous Media (Volume 8 of A Course of Theoretical Physics) Pergamon Press. 1960.